Pergamon

PII: S0045-7949(96)00362-8

Computers & Structures Vol. 63, No. 3, pp. 429–437, 1997

0045-7949/97 $17.00 + 0.00

SIZE EFFECTS IN BRITTLE SPECIMEN WITH MICROCRACK INTERACTION

Alberto Carpinteri and **Guoping Yang**
Department of Structural Engineering, Politecnico di Torino, 10129 Torino, Italy

(*Received* 22 *November* 1995)

Abstract—A numerical micromechanics model to simulate the failure process of finite sized brittle specimen with random interacting microcracks is proposed in this paper. The model combines the closed form crack solutions with boundary element method. Strength size effect is studied through the computational results from varied specimen sizes with different crack size distributions, from complete randomness to deterministic situations. The results reasonably explain why the size effect prevails in brittle materials containing disordered microimperfections. The more disordered crack size distribution provides lower strength and stronger strength size effect. © 1997 Elsevier Science Ltd. All rights reserved.

1. INTRODUCTION

Size effect on the strength of brittle materials is well known in civil engineering. Many explanations for size effect have been put forward, among which a well-known one is the "weakest links" theory by Weibull [1]. Much of the research work on size effects is the fitting of experimental results, and the conclusions obtained are not always accepted. The size effect rises originally from the microstructures of brittle materials, i.e. from the pre-existing imperfections in matrix or at the interface between matrix and aggregate. During the loading process, these micro-imperfections interact with finite sized boundaries, apart from crack interaction themselves. This mechanism leads to damage accumulation and causes the specimen failure. It can be very helpful to study the size effect with numerical micromechanics models including the crack interaction.

Many researches have been carried out on fracture behavior of brittle materials with interacting microcracks [2–4], but almost all of them are based on the infinite size case, without considering the boundary influence on the fracture behavior. In real situations, however, brittle materials present finite sized boundaries; the remarkable influence of the specimen size on the loading capacity should be considered.

In this paper, the strength size effect on specimen scaling is studied by a numerical micromechanics model for finite sized brittle specimens with random interacting microcracks. The whole failure process of finite sized specimen with interacting microcracks is simulated by combining the closed form crack solutions with boundary element method. Based on our previous microcrack interaction model in infinite sized plate [5–7], a fictitious stress boundary element is introduced to take into account the effects of finite sized boundaries. The brittle specimen is represented with an arbitrarily sized plate with a multitude of randomly distributed microcracks. Different microcrack size distributions (uniform and self-similar) are adopted. The load is divided into some increments; in each load increment the microcrack interaction and propagation and the influence of finite boundary on the fracture behavior of microcracks are followed progressively. During crack propagation, microcracks may coalesce and intersect each other, and some minor microcracks will be arrested, so a coalescence criterion is proposed to check the intersection and crack arrest behavior. To judge whether the specimen is in its failure stage, a coalescence matrix is utilized which allows us to recognize the fatal coalescence cluster out of many intersection groups of propagating microcracks. The numerical results from different specimen sizes can explain why the size effect emerges in brittle materials containing disordered microimperfections.

2. SIF EVALUATION AND CRACK PROPAGATION

It is convenient to adopt the fictitious stress concept for the computation of the stress intensity factors (SIFs) with interacting cracks. The fictitious stresses are assumed as the on-site stresses acting on the microcrack surfaces and producing the same SIFs as those from remote boundary stresses.

After solving the crack interaction problem, from the fictitious stresses on each microcrack determined at a certain loading increment, the SIFs can be

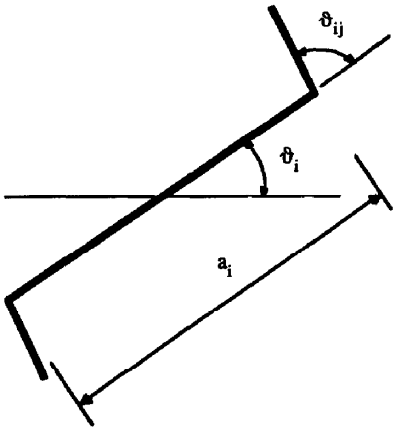

Fig. 1. Preexisting crack in mixed mode loading condition.

evaluated from

$$K_{\mathrm{I}}(\pm c) = \frac{1}{\sqrt{\pi c}} \int_{-c}^{c} \sigma_n \sqrt{\frac{c \pm x}{c \mp x}}\, \mathrm{d}x \tag{1a}$$

$$K_{\mathrm{II}}(\pm c) = \frac{1}{\sqrt{\pi c}} \int_{-c}^{c} \sigma_t \sqrt{\frac{c \pm x}{c \mp x}}\, \mathrm{d}x \tag{1b}$$

where c is the half-length of the crack, $K_{\mathrm{I}}(\pm c)$ and $K_{\mathrm{II}}(\pm c)$ are the SIFs at the two crack tips corresponding to Mode I and Mode II, respectively, σ_n and σ_t are the normal and shearing fictitious stresses taking into account crack interaction and finite sized boundary influences.

Suppose that there is only a preexisting crack of length a_i in mixed mode loading condition as shown in Fig. 1. From the well-known maximum hoop stress criterion, the crack tip $j (j = 1, 2)$ will start propagating when

$$\cos\frac{\theta_{ij}}{2}\left[K_{\mathrm{I}} \cos^2\frac{\theta_{ij}}{2} - \frac{3}{2} K_{\mathrm{II}} \sin\theta_{ij}\right] = K_{\mathrm{IC}} \tag{2}$$

where K_{IC} is the Mode I fracture toughness of the material and θ_{ij} is the propagation angle. The latter value, corresponding to the tip j of the crack i, satisfies the condition

$$K_{\mathrm{I}} \sin\theta_{ij} + K_{\mathrm{II}}(3\cos\theta_{ij} - 1) = 0. \tag{3}$$

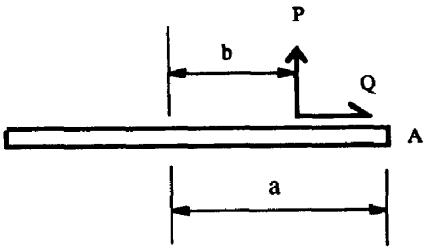

Fig. 3. Analogous problem for the case of Fig. 2.

When the microcrack interaction effect is not considered, the two angles θ_{i1} and θ_{i2} are equal, whereas these two values may differ from each other if crack interaction effect is included.

Now, if the primitive crack has propagated with two branching cracks, as shown in Fig. 2, the fictitious stresses σ and τ on the surfaces of the primitive crack, generated by the applied boundary stresses and crack interaction, result in an opening force O and a sliding force S on the branching cracks:

$$O = \begin{cases} a_i(-\tau \sin\theta_{ij} + \sigma\cos\theta_{ij}), & \text{for } \sigma > 0 \\ a_i(-\tau\sin\theta_{ij} + \sigma\lambda|\sin\theta_{ij}|), & \text{for } \sigma < 0 \end{cases} \tag{4a}$$

$$S = a_i(\tau + \sigma\lambda)\cos\theta_{ij} \tag{4b}$$

where λ is the friction coefficient between the two crack surfaces in compression. When the normal stress is positive, the frictional term in the preceding equations is absent.

For the computation of the SIFs at each tip of the branching cracks, an analogous problem, where an opening force P and a sliding force Q act on a crack

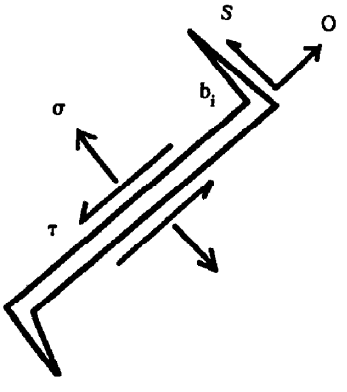

Fig. 2. Primitive crack with two branching cracks.

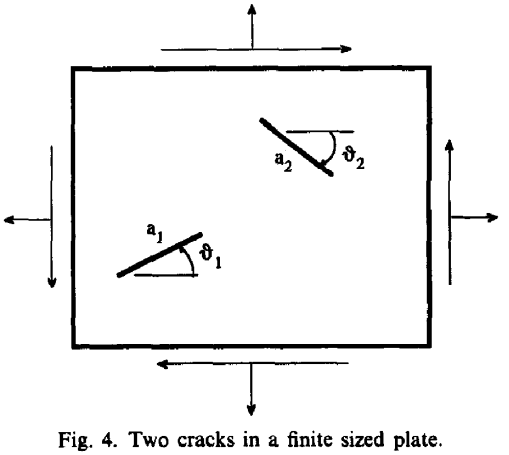

Fig. 4. Two cracks in a finite sized plate.

surface (Fig. 3), has to be considered:

$$K_{\mathrm{I}}^{A} = \frac{1}{2\sqrt{\pi a}}\left[P\sqrt{\frac{a+b}{a-b}} + Q\left(\frac{e-1}{e+1}\right)\right] \quad (5a)$$

$$K_{\mathrm{II}}^{A} = \frac{-1}{2\sqrt{\pi a}}\left[P\left(\frac{e-1}{e+1}\right) - Q\sqrt{\frac{a+b}{a-b}}\right]. \quad (5b)$$

The constant e depends on the material properties and the stress state in the specimen. In the case of a pair of opening forces, the SIFs at the tip are evaluated from

$$K_{\mathrm{I}} = \frac{O}{\sqrt{\pi b_i}} + \sigma_n\sqrt{\pi b_i} \quad (6a)$$

$$K_{\mathrm{II}} = \frac{S}{\sqrt{\pi b_i}} + \sigma_t\sqrt{\pi b_i} \quad (6b)$$

where b_i is the length of the branching crack, σ_n and σ_t are the fictitious normal and shearing stresses on it.

If σ_n is positive, the propagation length should be determined from

$$\frac{a_i(-\tau\sin\theta_{ij} + \sigma\cos\theta_{ij})}{\sqrt{\pi b_i}} + \sigma_n\sqrt{\pi b_i} = K_{\mathrm{IC}}. \quad (7)$$

If the major stress is compressive, the fictitious normal stress on primitive crack is negative in most cases,

$$S = \begin{cases} a_i(\tau + \sigma\lambda)\cos\theta_{ij}, & \text{for } \tau > 0 \\ a_i(\tau - \sigma\lambda)\cos\theta_{ij}, & \text{for } \tau < 0 \end{cases} \quad (8a)$$

$$O = a_i(-\tau\sin\theta_{ij} + \sigma\lambda|\sin\theta_{ij}|. \quad (8b)$$

If the fictitious normal stress on branching crack is also negative, then from

$$\frac{a_i(-\tau\sin\theta_{ij} + \sigma|\sin\theta_{ij}|)}{\sqrt{\pi b_i}} = K_{\mathrm{IC}} \quad (9)$$

we know that the propagation of the branching crack is stable, so its length can be obtained step by step with the increase of the applied external stresses on the specimen.

3. MICROCRACK INTERACTION

3.1. *Interaction between primitive straight cracks*

To consider crack interaction, stress field at the crack tip is needed. For the stress distribution around a crack whose surfaces are subjected to constant normal and shear stresses, Sneddon and Lowengrub [8] obtained closed form solutions. These exact solutions have been used to compute the SIFs of the microcracks with interaction effects [5, 6].

Two algorithms are herein adopted for computing the SIFs of interacting microcracks with and without propagation, respectively. The exact solutions from Sneddon and Lowengrub are used for primitive microcracks (not propagated), which allows us to get better estimations for the crack propagation initiation and branching directions. After the crack has propagated, the approximate K-dominant stress field, commonly used in classical fracture mechanics, is adopted for the computation of the stresses generated by the branching crack tips.

If an external stress field is applied to the specimen, the fictitious stress σ_{mi} on the surfaces of the microcracks is composed of two parts

$$\sigma_{mi} = \sigma_{mi}^{\mathrm{bound}} + \sigma_{mi}^{\mathrm{inter}}. \quad (10)$$

The first term, $\sigma_{mi}^{\mathrm{bound}}$, is the stress generated by the boundary stresses, while the second term, $\sigma_{mi}^{\mathrm{inter}}$, is the additional stress generated by the microcrack interaction. These two parts can be found out after solving the problem. We will focus our attention on the second part due to crack interaction effects, whereas the first part will be discussed in the following section within the boundary element method framework.

Considering boundary effects and crack interactions, the SIFs at the microcrack tips can be expressed as

$$K_{\mathrm{I}} = K_{\mathrm{I}}^{\mathrm{O}} + K_{\mathrm{I}}^{\mathrm{Add}} \quad (11a)$$

$$K_{\mathrm{II}} = K_{\mathrm{II}}^{\mathrm{O}} + K_{\mathrm{II}}^{\mathrm{Add}} \quad (11b)$$

in which K^{O} and K^{Add} are the SIFs corresponding to the applied boundary stresses and to the additional stresses generated by the crack interaction, respectively.

Just two microcracks are considered to make the formulation of crack interaction clearer. Let us assume two microcracks with arbitrary sizes and orientations a_1, a_2, θ_1, θ_2, as shown in Fig. 4, with a set of boundary stresses acting on the specimen. This fundamental problem can be decomposed into three sub-problems as shown in Fig. 5, where subscripts 1 and 2 represent microcrack 1 and 2, respectively. Stresses $\sigma_1^{\mathrm{bound}}$ and $\sigma_2^{\mathrm{bound}}$ are induced by the boundary stresses, while σ_{12} is the stress vector acting on microcrack 1 induced by microcrack 2. The surfaces of the latter are subjected to the stress vector $-(\sigma_2^{\mathrm{bound}} + \sigma_{21})$, where σ_{21} is the stress induced by microcrack 1 on microcrack 2. The surfaces of the former, on the other hand, are subjected to the stress vector $-(\sigma_1^{\mathrm{bound}} + \sigma_{12})$.

The problem focuses on finding these stress vectors caused by the boundary stresses and the interaction effects between the two cracks. If the final fictitious

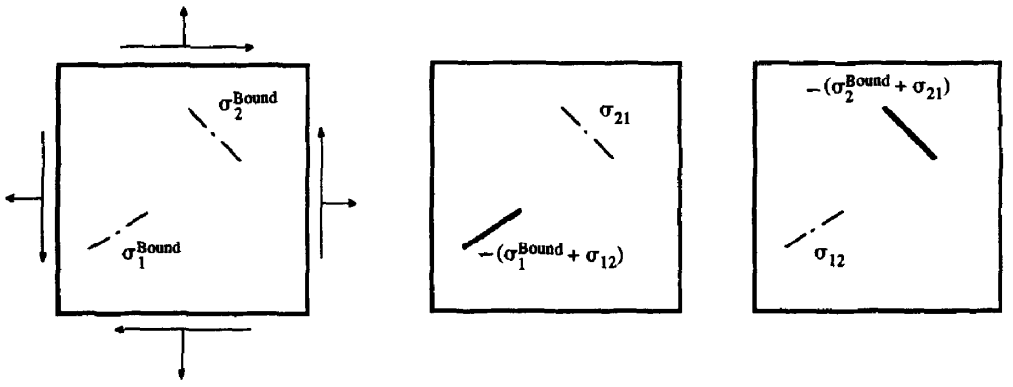

Fig. 5. Decomposition of the problem in Fig. 4.

normal stress and shear stress on microcrack 1 are denoted, on the crack line coordinate $x1$, as $p1(x1)$ and $s1(x1)$,

$$p1(x1) = -p1^{\text{bound}} - n1 \cdot \sigma_{12} \cdot n1 \quad (12a)$$

$$s1(x1) = -s1^{\text{bound}} - n1 \cdot \sigma_{12} \cdot t1 \quad (12b)$$

where $p1^{\text{bound}}$ and $s1^{\text{bound}}$ are the normal and shear stresses induced by the boundary load, $n1$ and $t1$ are direction cosines of microcrack 1. The stresses $p2(x2)$ and $s2(x2)$ on the surface of microcrack 2 are analogously given by

$$p2(x2) = -p2^{\text{bound}} - n2 \cdot \sigma_{21} \cdot n2 \quad (13a)$$

$$s2(x2) = -s2^{\text{bound}} - n2 \cdot \sigma_{21} \cdot t2 \quad (13b)$$

where $n2$ and $t2$ are the direction cosines of microcrack 2. Let us distinguish the individual contributions of normal and shear stresses to the additional stress vectors

$$\sigma_{12} = k_{12}^{p} \cdot p2(x2) + k_{12}^{s} \cdot s2(x2) \quad (14a)$$

$$\sigma_{21} = k_{21}^{p} \cdot p1(x1) + k_{21}^{s} \cdot s1(x1) \quad (14b)$$

in which k_{12}^{p}, k_{12}^{s}, k_{21}^{p}, k_{21}^{s} are influence vectors corresponding to the stress field generated by unit normal or shear stresses on the interacting microcrack. The stresses $p1$, $s1$, $p2$, $s2$ can be expressed as

$$p1 = -p1^{\text{bound}} - R_{12}^{pp} \cdot p2 - R_{12}^{ps} \cdot s2 \quad (15a)$$

$$s1 = -s1^{\text{bound}} - R_{12}^{sp} \cdot p2 - R_{12}^{ss} \cdot s2 \quad (15b)$$

$$p2 = -p2^{\text{bound}} - R_{21}^{pp} \cdot p1 - R_{21}^{ps} \cdot s1 \quad (15c)$$

$$s2 = -s2^{\text{bound}} - R_{21}^{sp} \cdot p1 - R_{21}^{ss} \cdot s1 \quad (15d)$$

where R_{12}^{pp}, R_{12}^{ps}, R_{12}^{sp}, R_{12}^{ss}, . . ., represent the interaction coefficients between two microcracks.

Let us extend the procedure to the multi-microcrack situation. If there are M microcracks in the specimen, the problem can thus be decomposed into $M + 1$ sub-problems following the same formulation steps as those in the case of two microcracks,

$$pi = -pi^{\text{bound}} - \sum_{k \neq i}^{M} [R_{ik}^{pp} \cdot pk + R_{ik}^{ps} \cdot sk] \quad (16a)$$

$$si = -si^{\text{bound}} - \sum_{k \neq i}^{M} [R_{ik}^{sp} \cdot pk + R_{ik}^{ss} \cdot sk]. \quad (16b)$$

Equation (16) represents $2M$ linear relations for solving $2M$ unknowns $p1$, $s1$, . . . , pm, sm. In the next section 6 degrees of freedom will be used to represent the stress state of a crack during propagation.

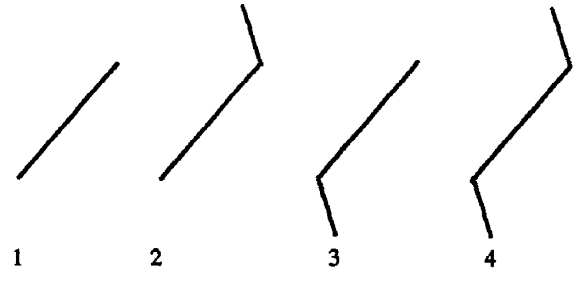

Fig. 6. Different crack patterns during propagation.

3.2. *Crack interaction during propagation*

Microcracks configurations during propagation can be grouped into four types as shown in Fig. 6, according to the possible different branching situations. In the formulation procedure, the two main steps are given by the different treatments of stresses on the microcrack (referred to as target microcrack) caused by other interaction microcracks (referred to as source microcracks), and the evaluation of the stress field generated by source microcracks.

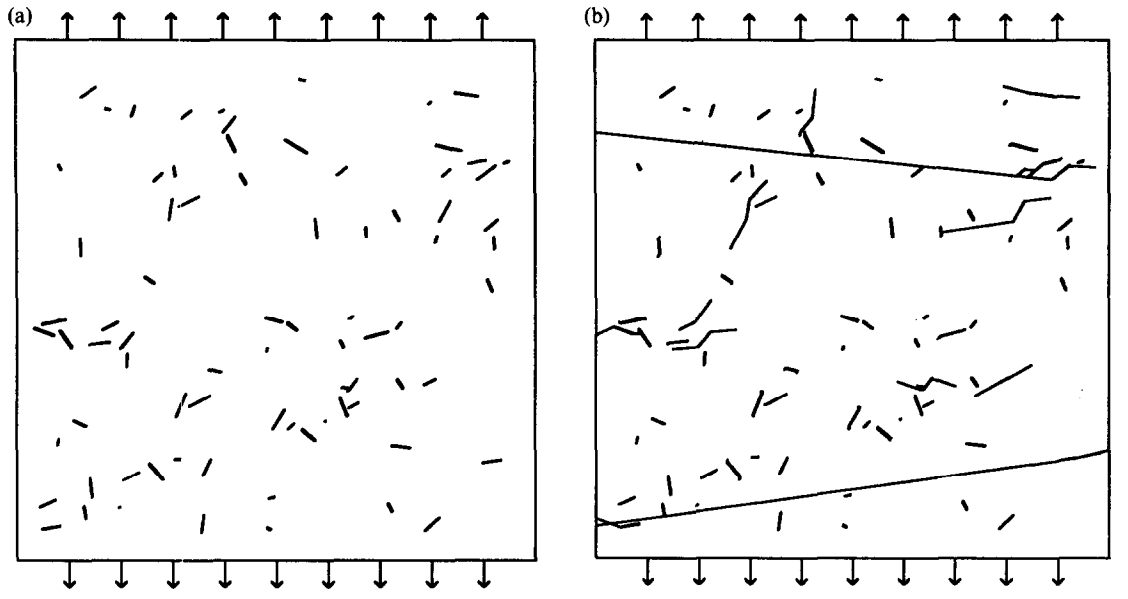

Fig. 7. (a) Primitive crack distribution in tension (uniform crack size distribution); (b) crack pattern at failure of the specimen shown in (a).

For the evaluation of the stresses on a target microcrack generated by other source microcracks, normal and shear stresses at three locations on each target microcrack are computed so as to obtain the SIFs at two tips of the crack. The choice of the three points on target crack depends on the different propagation patterns of the crack. If the two crack tips have not propagated (type 1) the stresses at the three points can give out a quadratic stress distribution on the crack, which allow us to determine more accurately the initiation of the branching cracks. If only one tip of the primitive crack has propagated (type 2 or type 3), then a linearly varied stress distribution on the primitive crack is determined. In the case both tips have propagated (type 4), we get constant stress distribution on the primitive crack.

Since six stresses at three points on a microcrack must be always considered for different fracture situations, the characteristic matrix expressed in eqn (16) should be extended to be compatible with the 6 degrees of freedom for each microcrack. For the contribution of the source microcrack J to the stresses on the target microcrack I, the corresponding submatrix takes the following form

$$R_{I,J} == \begin{bmatrix} R_{6*I-5,6*J-5} & R_{6*I-5,6*J-4} & \cdots & \cdots & \cdots \\ R_{6*I-4,6*J-5} & R_{6*I-4,6*J-4} & \cdots & \cdots & \cdots \\ \cdots & \cdots & \cdots & \cdots & \cdots \\ \cdots & \cdots & \cdots & R_{6*I,6*J-1} & R_{6*I,6*J} \end{bmatrix} . \quad (17)$$

The interaction matrix is thus $6M*6M$ when M microcracks are present in the specimen. Combining this matrix with the boundary elements described in the sequel, final fictitious stresses on each microcrack can be obtained after solving the interaction problem. The propagation conditions and the lengths of the branching cracks can then be computed or checked according to the above criteria, step by step along with the increment of the external loads.

4. FINITE SIZED BOUNDARY INFLUENCE

The previous formulation procedures are based on the solution of cracks in an infinite elastic domain. To take into account the influence of finite sized boundary, a boundary element method is introduced. The framework of fictitious stress method (FSM) [9, 10] is in accordance with the previous formulations since in both of them the unknowns are the stresses deduced from the other stress sources.

FSM is based on the exact solution of a point force acting on an elastic field. A fictitious stress is assumed to act on the discrete boundary element, which is called stress discontinuity (SD) element since there exists a stress jump on both sides of the element. Over each element, the stress discontinuities are assumed to vary according to a given mode (constant, linear, etc.). The normal and shear stresses pi and si generated by N discrete SD elements are

$$pi = \sum_{j=1}^{N} C_{ij}^{pp} pj + \sum_{j=1}^{N} C_{ij}^{ps} sj \quad (18a)$$

$$si = \sum_{j=1}^{N} C_{ij}^{sp} pj + \sum_{j=1}^{N} C_{ij}^{ss} sj \tag{18b}$$

where pj, sj are the unknown normal and shear stress discontinuities at the mid-point of the boundary element j, C_{ij}^{pp}, C_{ij}^{ps}, etc. are the influence coefficients of stresses at point j on those at point i.

In the case of cracks in a finite sized body, we can divide the external boundary into N stress discontinuity elements, which, with M internal microcracks, provide the following $2N + 6M$ algebraic equations:

$$pi = -\sum_{j=1}^{N} [C_{ij}^{pp} pj + C_{ij}^{ps} sj] - \sum_{k \neq i}^{M} \sum_{l=1}^{3} [R_{ikl}^{pp} \cdot pk_l + R_{ikl}^{ps} \cdot sk_l] \tag{19a}$$

$$si = -\sum_{j=1}^{N} [C_{ij}^{sp} pj + C_{ij}^{ss} sj] - \sum_{k \neq i}^{M} \sum_{l=1}^{3} [R_{ikl}^{sp} \cdot pk_l + R_{ikl}^{ss} \cdot sk_l] \tag{19b}$$

which enables us to determine $2N$ stress discontinuity unknowns and $6M$ fictitious stresses for M microcracks, and thus to evaluate the SIFs at each microcrack tip with different propagation configurations in a finite sized plate.

5. CRACK PROPAGATION VS ARREST AND FAILURE CRITERION

During crack propagation, some branching cracks may intersect with other cracks, so it is necessary to set up the criterion for finding the intersection locations. When the intersection takes place, there will be two possible cases in computer simulation within a certain load increment. The first case is that the propagating crack tip is very close to another crack within a given distance (in computation we use 0.1 mm), the second one is that the propagating crack tip passes across another crack. From experimental observations, we know that some minor cracks will stop propagating when they intersect with other cracks (so-called *crack arrest*). Therefore at each load increment, we compute the new positions of the propagating crack tips: if intersection occurs, the shorter branching crack will stop propagating, whereas the longer one can continue propagating in the next load increment. In the case where two branching cracks pass across each other, the propagating length of the shorter branching crack should be modified by the intersection position.

Since the algorithm used in this study is step by step in load increment, the specimen failure should be checked at each load increment. Many crack intersections arise during propagation in a very dense microcrack array, and also many intersections coalesce each other. So it is rather difficult to identify how many independent intersection clusters exist at a certain load step. A coalescence matrix is adopted to identify the independent coalescence clusters. The element $c_{i,j}$ in the coalescence matrix represents the intersection state between the microcracks i and j, whose value is unity when these two cracks intersect each other, while it is zero with no intersection. From this matrix, different independent intersection clusters can be determined, and each independent cluster is checked against the global failure of the specimen. If an independent crack coalescence cluster intersects with two terminal boundary elements, the specimen is assumed to fail, and this cluster is assumed to be fatal.

6. SIZE EFFECTS OF BRITTLE MATERIALS

For the microcrack distribution in brittle materials, the crack density and the possible maximum crack size are the most important microstructure parameters. Taking concrete as an example, the crack density is connected with many factors such as the cement type, mixture properties, process method and so on. The possible maximum crack size, on the other hand, is usually determined by the maximum aggregate size. The equal crack density assumption is adopted, while the possible maximum crack size is the same for different specimen sizes.

For all the cases studied, four different sized specimens are computed. The square specimen sides are 50, 75, 100 and 150 mm, respectively. The material parameters are: Young's modulus $E = 30{,}000\ \mathrm{Nmm^{-2}}$; Poisson ratio $\nu = 0.3$; fracture toughness $K_{IC} = 20\ \mathrm{Nmm^{-3/2}}$. Independent uniform distributions for the position and orientation of microcracks in the specimen are adopted. It should be noted that the different combinations of crack position and orientation will give out different internal microstructures. In the examples, 10 samples for each combination of position and orientation are computed, and the average loads are considered for size effects.

To keep the crack density unchanged, the numbers of the randomly distributed microcracks are taken as 20, 45, 80 and 180, respectively, for the four different specimen sizes. The possible maximum crack size is assumed to be 5 mm in each case. Uniform distribution and other disordered assumptions in crack size variation, are studied.

6.1. *Uniform crack size distribution*

The crack sizes are assumed with uniform distribution within the range between 0 and 5 mm. The average failure loads in uniaxial tension are 4.550, 3.150, 2.800 and 2.625 $\mathrm{Nmm^{-2}}$, respectively.

The primitive crack distribution in the 100 mm specimen is shown in Fig. 7(a), and the crack pattern at failure stage is shown in Fig. 7(b). The linear regression relation in bilogarithmic form is

$$\text{Log}(\sigma) = 3.372 - 0.495\,\text{Log}(s) \qquad (20)$$

in which σ is the failure stress (in Nmm^{-2}), and s is the specimen side (in mm).

With the same specimen parameters, the uniaxial compressive failure loads are -25.780, -16.000, -15.110 and $-12.500\ \text{Nmm}^{-2}$, respectively. The linear regression relation is

$$\text{Log}(\sigma) = 5.624 - 0.629\,\text{Log}(s). \qquad (21)$$

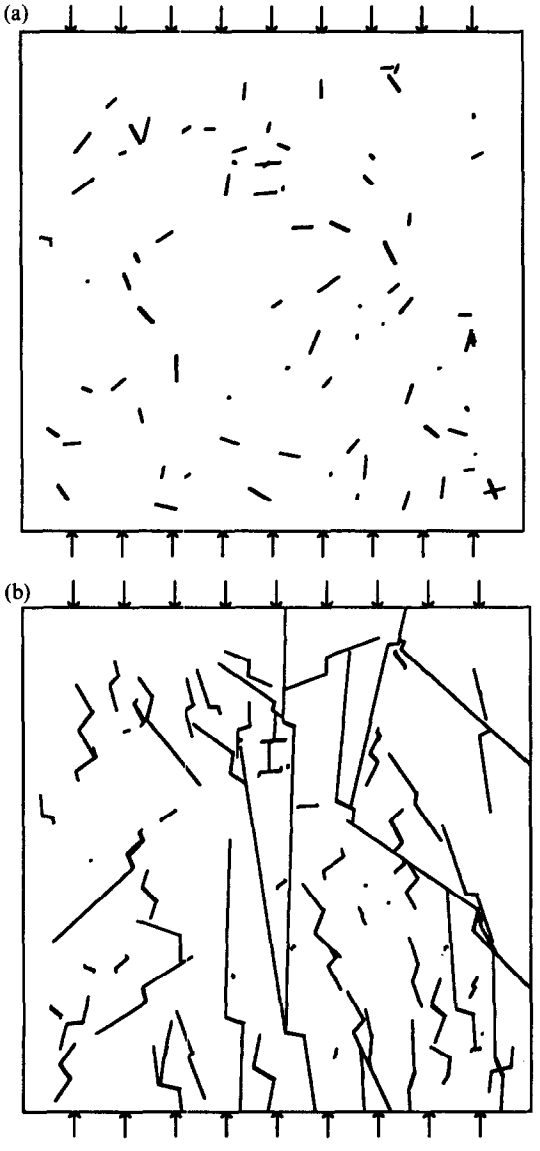

Fig. 8. (a) Primitive crack distribution in compression (uniform crack size distribution); (b) crack pattern at failure of the specimen shown in (a).

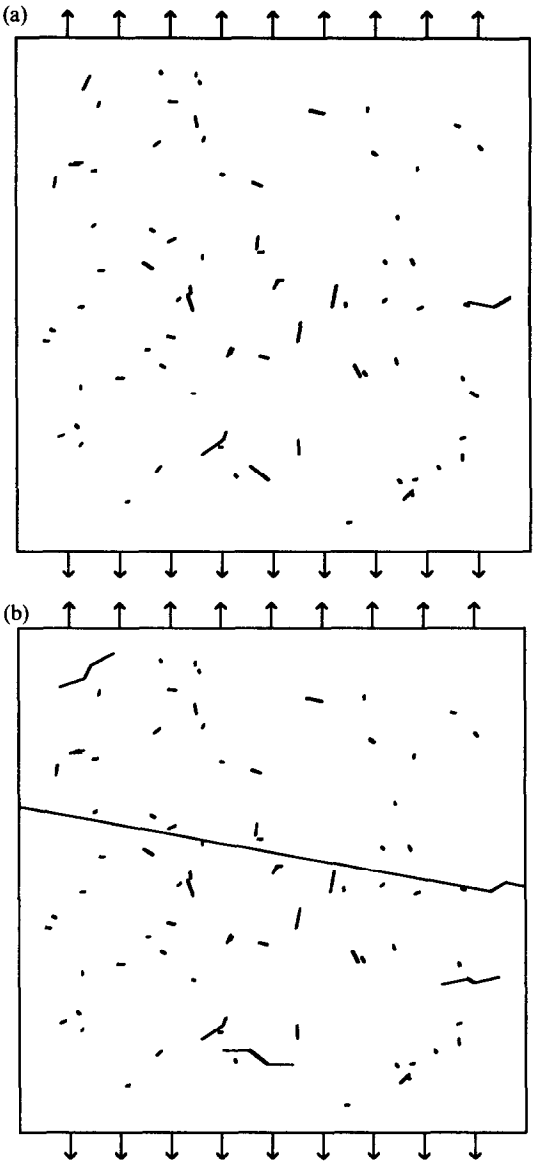

Fig. 9. (a) Primitive crack distribution in tension (self-similar crack size distribution); (b) crack pattern at failure load in tension (self-similar crack size distribution).

The primitive microcrack distribution with specimen size 100 mm in compression is shown in Fig. 8(a), whereas the final crack pattern is shown in Fig. 8(b).

6.2. *Self-similar crack size distribution*

If a general disordered distribution for microcrack size is assumed [11], the microcrack size a varies with the probability density

$$p(a) = \frac{NC}{a^{N+1}} \qquad (22)$$

in which N is an "order parameter" to measure the degree of disorder in the materials (larger values of N correspond to more ordered distributions in crack

Table 1. Failure stresses with variation of the "order parameter"

	$s = 50$ mm ($\mathrm{Nmm^{-2}}$)	$s = 75$ mm ($\mathrm{Nmm^{-2}}$)	$s = 100$ mm ($\mathrm{Nmm^{-2}}$)	$s = 150$ mm ($\mathrm{Nmm^{-2}}$)
$N = 10$	7.850	7.225	6.675	6.350
$N = 4$	7.475	6.725	6.375	5.775
$N = 1$	5.950	5.200	3.775	3.625

length variation). When N approaches infinity, we get a constant crack size distribution. C is a constant determined by the minimum and maximum microcrack lengths, by the number of the cracks and by the value of N. For example, if the minimum and maximum crack lengths in the specimen are $a_{\min}$, $a_{\max}$, respectively, the number of microcracks is

$$n_t = \int_{a_{\min}}^{a_{\max}} \frac{NC}{x^{N+1}}\,\mathrm{d}x = C\left[\frac{1}{a_{\min}^N} - \frac{1}{a_{\max}^N}\right]. \tag{23}$$

We assume $a_{\min} = 0.5$ mm, $a_{\max} = 5$ mm. At first, we consider the case corresponding to the more ordered situation, $N = 10$. The computed average failure loads in tension are 7.850, 7.225, 6.675 and 6.350 $\mathrm{Nmm^{-2}}$, respectively. The linear regression relation in bilogarithmic form is

$$\mathrm{Log}(\sigma) = 2.831 - 0.198\,\mathrm{Log}(s). \tag{24}$$

When $N = 4$, we have a more disordered crack size distribution. Again the same specimen sizes and material parameters are adopted. The average failure loads in tension are 7.475, 6.725, 6.375 and 5.775 $\mathrm{Nmm^{-2}}$, respectively. The linear regression relation in bilogarithmic form is

$$\mathrm{Log}(\sigma) = 2.915 - 0.232\,\mathrm{Log}(s). \tag{25}$$

When $N = 1$, we have a self-similar distribution for microcrack size [11], which is the most disordered. One of the primitive crack distributions with the 100 mm specimen side is shown in Fig. 9(a), and the related failure crack pattern is shown in Fig. 9(b). The average failure loads in tension are 5.950, 5.200, 3.775 and 3.625 $\mathrm{Nmm^{-2}}$, respectively. The linear regression relation in bilogarithmic form is

$$\mathrm{Log}(\sigma) = 3.714 - 0.494\,\mathrm{Log}(s). \tag{26}$$

Computed results of the failure stresses with the variation of the "order parameter" N are grouped in Table 1.

It can be found from Table 1 that the failure stresses increase with the increment of the "order parameter" N. For example, the failure stresses for the specimen sized 50 mm are 7.850, 7.475 and 5.950 $\mathrm{Nmm^{-2}}$, respectively, when N decreases from 10 to 1. It means that the more ordered crack size distribution gives out higher strength.

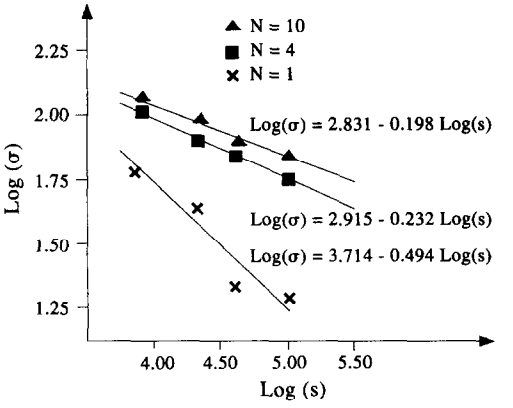

Fig. 10. Size effects for the generalized self-similar crack size distributions in tension.

Comparison between eqns (24)–(26) is shown in Fig. 10. We can observe that the absolute values of the slope in the bilogarithmic diagram increase with the decrease of the "order parameter" N. This means that the more ordered crack distribution corresponds to a weaker dependence of strength on the specimen size.

The slopes of the regression expressions of eqns (20) and (26) (the values are -0.495 and -0.494, respectively) are very close to $-1/2$, which is the classical stress-singularity power of linear elastic fracture mechanics.

7. CONCLUDING REMARKS

Coupling between crack interaction, propagation and finite sized boundary influences is considered, and a novel numerical micromechanics model to simulate the failure process of finite sized brittle specimen is proposed in this paper. The model combines the closed form crack solutions with boundary element method. A coalescence criterion is adopted to check the intersection behavior and propagation arrest. A coalescence matrix can identify the fatal coalescence cluster out of many intersections of propagating microcracks.

Strength size effect with specimen scaling is studied through the numerical results from varied specimen sizes, with the uniform distribution and general disordered assumptions in equal crack density with fixed possible maximum crack length. It is very interesting that almost the same size effects are found for two different crack size distributions in tension. The slopes of the bilogarithmic diagram are nearly equal to $-1/2$, which is just the classical stress-

singularity power of linear elastic fracture mechanics. It is found that the more ordered crack size distribution provides higher strength and weaker size effect.

REFERENCES

1. W. Weibull, *A Statistical Theory for the Strength of Materials*. Swedish Royal Institute for Engineering Research, Stockholm (1939).
2. H. Horii and S. Nemat-Nasser, Brittle failure in compression: splitting, faulting and brittle-ductile transition. *Phil. Trans. R. Soc. London*, **A 319,** 337–374 (1986).
3. M. Kachanov, Elastic solids with many cracks: a simple method of analysis. *Int. J. Solids Struct.* **23,** (1) 23–43 (1987).
4. L. R. F. Rose, Microcrack interaction with a main crack. *Int. J. Fracture*, **31,** 233–242 (1986).
5. Guo-ping Yang and Xila Liu, Microcrack interaction in concrete. *Proc. Intl. Symp. on Concrete Engng.*, Nanjing (1991).
6. Guo-ping Yang and Xila Liu, Interaction and propagation of random microcracks in compression. *Studi e Ricerche, Italy*, **14,** 121–141 (1993).
7. A. Carpinteri and Guo-ping Yang, Fractal dimension evolution of microcrack net in disordered materials. *Theor. appl. Fracture Mech.* **25,** 73–81 (1996).
8. I. N. Sneddon and M. Lowengrub, *Crack Problems in The Classical Theory of Elasticity*. Wiley, New York (1969).
9. S. L. Crouch and A. M. Starfield, *Boundary Element Methods in Solid Mechanics*. George Allen and Unwin, London (1983).
10. A. Carpinteri, C. Scavia and G. P. Yang, Microcrack propagation, coalescence and size effects in compression. *Engng Fracture Mech.* **54,** 335–347 (1996).
11. A. Carpinteri, Scaling laws and renormalization groups for strength and toughness of disordered materials. *Int. J. Solids Struct.* **31,** 291–302 (1994).